JOURNAL OF BACTERIOLOGY, July 2011, p. 3342–3355 Vol. 193, No. 13
0021-9193/11/$12.00 doi:10.1128/JB.00328-11

Binding and Spreading of ParB on DNA Determine Its Biological Function in *Pseudomonas aeruginosa*▽†

Magdalena Kusiak,[1] Anna Gapczyńska,[1] Danuta Płochocka,[1] Christopher M. Thomas,[2] and Grażyna Jagura-Burdzy[1]*

The Institute of Biochemistry and Biophysics, PAS, 02-106 Warsaw, Pawińskiego 5A, Poland,[1] and School of Biosciences, The University of Birmingham, Edgbaston, Birmingham B15 2TT, United Kingdom[2]

Received 8 March 2011/Accepted 15 April 2011

ParB protein of *Pseudomonas aeruginosa* belongs to a widely represented ParB family of chromosomally and plasmid-encoded partitioning type IA proteins. Ten putative *parS* sites are dispersed in the *P. aeruginosa* chromosome, with eight of them localizing in the *oriC* domain. After binding to *parS*, ParB spreads on the DNA, causing transcriptional silencing of nearby genes (A. A. Bartosik et al., J. Bacteriol. 186:6983–6998, 2004). We have studied ParB derivatives impaired in spreading either due to loss of DNA-binding ability or oligomerization. We defined specific determinants outside of the helix-turn-helix motif responsible for DNA binding. Analysis confirmed the localization of the main dimerization domain in the C terminus of ParB but also mapped another self-interactive domain in the N-terminal domain. Reverse genetics were used to introduce five *parB* alleles impaired in spreading into the *P. aeruginosa* chromosome. The single amino acid substitutions in ParB causing a defect in oligomerization but not in DNA binding caused a chromosome segregation defect, slowed the growth rate, and impaired motilities, similarly to the pleiotropic phenotype of *parB*-null mutants, indicating that the ability to spread is vital for ParB function in the cell. The toxicity of ParB overproduction in *Pseudomonas* spp. is not due to the spreading since several ParB derivatives defective in oligomerization were still toxic for *P. aeruginosa* when provided in excess.

Accurate segregation of genomes is important for genetic stability. The prokaryotic DNA partitioning process is best understood for low-copy-number plasmids. It relies on two partitioning proteins, A and B, and a *cis*-acting centromere-like sequence (*parS*), specifically recognized by the B component. Protein A with a weak NTPase activity forms dynamic spatial structures, and the interactions between protein A and protein B bound to DNA facilitate the separation and the movement of plasmid molecules to opposite poles before cell division (13). Plasmid partitioning operons are classified into four different groups (I to IV) based on the type of NTPase (Walker-type ATPase, actin-like ATPase, and tubulin-like GTPase), DNA-binding protein structure, and localization of *parS* (12, 13, 17, 29, 51). The majority of bacterial chromosomes encode ParA-ParB systems classified as IA on the basis of possession of ParA Walker-type ATPase and ParB, a large DNA-binding protein with an helix-turn-helix (H-T-H) motif. The multiple copies of the highly conserved *parS* sequence are dispersed throughout the chromosomes (34, 55). Despite the conservation in the binding sites and overall homology of chromosomal Par proteins, the effects of *par* deficiencies are genus specific. The effects range from lethality in *Caulobacter crescentus* (34, 39), to impairments in cell cycle regulation, chromosome segregation, and sporulation processes in *Streptomyces coelicolor* and *Bacillus subtilis* (8, 19, 23, 24, 31, 36), to mild defects in chromosome segregation at a specific growth phase in *Pseudomonas putida* (14, 33).

We are interested in the chromosome partitioning process in the opportunistic pathogen *Pseudomonas aeruginosa*. It encodes the *parA-parB* operon in the proximity of *oriC*. Ten putative *parS* sequences are dispersed in the *P. aeruginosa* chromosome, with eight of them localizing in the *oriC* domain (20% of the nucleoid around *oriC*). The *parA*- or *parB*-null mutants exhibit pleiotropic phenotypes: slower growth rate, increase in cell size, frequent production of anucleate cells independently of the growth phase, and defects in swarming and swimming motilities (4, 30). The lack of one partner increases the susceptibility of another for proteolytic degradation, making it difficult to separate the roles of individual proteins. However, some *parB* mutants with short deletions (e.g., H-T-H motif) produce normal levels of ParA and still demonstrate similar pleiotropic phenotypes, which strongly suggests that inactive ParB is the primary cause of the observed defects (4). The wide spectrum of *parB* deficiency effects suggests that ParB may play the regulatory role in the expression of different operons either through interaction with DNA or with other proteins, including ParA.

Chromosomally encoded ParBs belong to the highly homologous ParB family. ParBs of subtype IA (12) are relatively large proteins (300 to 400 amino acids) with a number of well-conserved motifs (5, 54). The H-T-H motif present in the middle of the proteins is involved in interactions with DNA (3, 5). The C-terminal dimerization domain with conserved region 4 (5) is the main dimerization domain (5, 10, 21, 52). The functions of the two motifs ParB box I and ParB box II (54), as well as those of three other regions (1 to 3), remain unspecified (5). The best-studied members of ParB family are the plasmid-

* Corresponding author. Mailing address: Institute of Biochemistry and Biophysics, PAS, 02-106 Warsaw, Pawińskiego 5A, Poland. Phone: 48 22 823 71 92. Fax: 48 22 658 46 36. E-mail: gjburdzy@ibb.waw.pl.

† Supplemental material for this article may be found at http://jb.asm.org/.

▽ Published ahead of print on 29 April 2011.

TABLE 1. Bacterial strains used in this study

Strain	Genotype[a]	Source or reference
Escherichia coli		
BL21(DE3)	F$^-$ *ompT hsdS*$_B$(r_B^- m_B^-) *gal dcm* (λDE3)	Novagen
DH5α	*recA1 endA1 gyrA96 thi-1 hsdR17*(r_K^- m_K^+) *supE44 relA1 deoR* Δ(*lacZYA-argF*)*U169* (ϕ80d*lacZ*ΔM15)	15
NR9786	Δ(*pro-lac*) *thi galK2*	R. Schaaper
S17-1	*pro* Δ*hsdR hsdM*$^+$ *recA*; Tp^r Sm^r ΩRP4-Tc::Mu-Kn::Tn*7*	50
Pseudomonas aeruginosa		
PAO1161	*leu* r$^-$	B. M. Holloway
PAO1161$_{Rif}$	*leu* r$^-$ Rif^r	4
PAO1161*parB*$_{null}$	*leu* r$^-$ Rif^r *parB* 1-18::TcR	4
PAO1161*parB*$_3$	*leu* r$^-$ Rif^r *parB* G289→A (ParB A97T)*	This study
PAO1161*parB*$_7$	*leu* r$^-$ Rif^r *parB* C473→T (ParB A158V)*	This study
PAO1161*parB*$_9$	*leu* r$^-$ Rif^r *parB* C280→T (ParB R94C)*	This study
PAO1161*parB*$_{55}$	*leu* r$^-$ Rif^r *parB* G211→A (ParB G71S)*	This study
PAO1161*parB*$_{62}$	*leu* r$^-$ Rif^r *parB* C494→T (ParB T165I)*	This study

[a] *, Amino acid substitutions in ParB protein derivatives are indicated in parentheses. Tp^r, trimethoprim resistance; Sm^r, streptomycin resistance, Rif^r, rifampin resistance; r$^-$, restriction-negative strain.

encoded ParB of P1 prophage (35, 53), KorB of RK2/RP4 plasmid (6, 21, 36), and SopB of F plasmid (1, 16, 37). The crystallographic studies have shown that ParB, KorB, and SopB interact with the specific DNA sequences *parS*, O_B, and *sopC*, respectively, in different ways. ParB of P1 recognizes a complex combination of heptameric and hexameric motifs in *parS* (A and B sequences) through two distinct DNA-binding domains: an H-T-H structure (A-box) and a new type of DNA-binding domain formed by dimerized C termini on DNA (B-box) (47). KorB of the RK2/RP4 plasmid (partition protein acting as the global transcriptional regulator) recognizes a simple palindromic motif of 13 bp, 12 copies of which are scattered through the plasmid genome. It has been concluded that although the H-T-H motif is the important determinant of operator O_B recognition, other residues downstream of H-T-H are also involved in specific DNA interactions (26). SopB of F plasmid, on the other hand, recognizes an 18-bp core of the 43-bp sequence directly repeated 12 times in the *sopC* region (40). SopB wrapped around DNA forms an extended partition complex with *sopC* in which the SopA interacting domains are aligned on one face of the complex (48). Although the primary dimerization domain of SopB was mapped to the C-terminal 48 residues (275 to 323), the crystal structure revealed the secondary dimerization domain to be located between residues 245 and 272. This secondary dimerization domain is supposed to be responsible for plasmid pairing and in *trans* spreading on the bridged DNA molecules (48). Superimposition of crystallographic data on SopB, ParB, and KorB in this region excluded the formation of such secondary dimerization domains in ParB of the P1 plasmid and KorB of the RK2/RP4 plasmid (48).

The unique feature of ParBs of type IA is the ability to spread on DNA starting from the specifically recognized sequence of *parS*, which may result in the transcriptional silencing of the nearby promoters (5, 7, 24, 35, 37, 44). The overproduction of $ParB_{Pa.}$ in *P. aeruginosa* and *P. putida* but not in *Escherichia coli* (one of the exceptions among bacteria since it does not possess a *par* system) is "toxic" for the cells since their division time becomes longer (5). One hypothesis was that toxicity might be the direct result of ParB spreading on DNA around multiple ParB binding sites (*parS*s) and silencing of important genes.

We describe here an analysis of *P. aeruginosa parB* mutants unable to spread and transcriptionally silence a promoter located close to *parS*. *In vitro* analysis of purified products of mutated alleles correlated the spreading deficiency either with impairment in DNA binding or with the ability to form higher-order structures. It allowed us to define the DNA-binding determinants outside of the H-T-H motif and demonstrate the role of N-terminal residues in the oligomerization process. Several ParB spreading-deficient derivatives are still toxic for *P. aeruginosa* if overproduced, indicating that DNA binding and spreading on DNA is not the main cause of toxicity. The introduction of analyzed mutant *parB* alleles with single nucleotide substitutions into the *P. aeruginosa* chromosome leads to phenotypes observed for a *parB*-null mutant, strongly suggesting that spreading on DNA starting from the *parS* sequences is required for the biological function of ParB in *P. aeruginosa*.

MATERIALS AND METHODS

Bacterial strains and growth conditions. Strains used in the present study are listed in Table 1. Bacteria were grown in L broth (25) at 37 or 30°C or on L agar (L broth with 1.5% [wt/vol] agar).The antibiotics used were as follows: benzylpenicillin (150 μg/ml in liquid medium and 300 μg/ml on agar plates), streptomycin (30 μg/ml), kanamycin (50 μg/ml), chloramphenicol (10 μg/ml in *E. coli* and 100 μg/ml in *P. aeruginosa*), carbenicillin (300 μg/ml), and rifampin (300 μg/ml). The L agar used for blue-white screening contained 0.1 mM IPTG (isopropyl-β-D-thiogalactopyranoside) and X-Gal (5-bromo-4-chloro-3-indolyl-β-D-galactopyranoside) at 40 μg ml^{-1}. MacConkey agar base supplemented with 2% galactose was used for screening of the Gal$^+$ phenotype. Growth was monitored by measurement of the optical density at 600 nm (OD_{600}).

Motility assays. For motility assays, cells of *P. aeruginosa* PAO1161 strains were taken from a deep-frozen stock spread on L-agar plates and grown overnight at 37°C. Bacteria from single colonies were then used to inoculate test plates (43). Plates were incubated for 24 h or 48 h either at 27 or 37°C. All sets of plates were standardized by using the same volume of medium.

Plasmids and DNA manipulations. The plasmids used in the present study are listed in Tables 2 and 3. Plasmid DNA isolation and genetic manipulations were based on standard techniques (45). Standard PCRs were performed on plasmid DNA templates with the mutated *parB* alleles using 2.5 pmol of the primers parB1 and parB2 (see Table S1 in the supplemental material). DNA sequencing was performed by the internal sequencing facility (Institute of Biochemistry and Biophysics, Warsaw, Poland) using the dye terminator method in conjunction with an ABI 373 automated DNA sequencer.

TABLE 2. Plasmids used in this study

Plasmid	Relevant features[a]	Source or reference
pABB811	pGB2 with $parS_2$ sequence (orientation I)	5
pAKE600	ori_{MB1} $oriT_{RK2}$; Ap^r *sacB*	11
pBBR1MCS1	BHR cloning vector *lacZ*α-MCS *mob* T7*p* T3*p*; Cm^r	28
pET28mod	ori_{MB1} Km^r, T7*p*, *lacO*, His tag, no BamHI site, T7 tag deleted	36
pGB2	ori_{SC101}; Sp^r/Sm^r	9
pGBT30	ori_{MB1}, Ap^r, $lacI^q$ *tacp* expression vector	22
pJMB500	pBBR1MCS1 with $tacp\text{-}parB_{Pa}$	30
pKLB2	pGBT30 with $tacp\text{-}parB_{Pa}$	5
pKLB3	pGBT30 with $tacp\text{-}parA\text{-}parB_{Pa}$	5

[a] Cm^r, chloramphenicol resistance; Sm^r, streptomycin resistance; Ap^r, ampicillin resistance; Sp^r, spectinomycin resistance; Km^r, kanamycin resistance.

PCR site-directed mutagenesis was used to obtain *P. aeruginosa parB* ($parB_{Pa}$) alleles with single amino acid substitutions in pMKB4, a pAKE600 derivative (11) (a modification of Stratagene QuikChange site-directed mutagenesis). Pairs of primers were designed to introduce the desired mutation and remove or introduce restriction site (without changing amino acid sequence) in close proximity to mutagenized sequence (see Table S1 in the supplemental material). The PCR amplification was performed according to the following thermocycler program: 30 s of initial denaturation at 95°C, followed by 16 cycles of denaturation at 95°C for 30 s, annealing at 55°C for 1 min, and elongation at 68°C for 16 min, with a final elongation step at 68°C for 30 min. After the temperature cycling, the product was treated with 10 U of DpnI endonuclease in order to digest the parental DNA template and used for transformation. The plasmid DNA was sequenced to verify the presence of the mutation.

***E. coli* and *P. aeruginosa* transformation.** Competent cells of *E. coli* were prepared by the standard $CaCl_2$ method (45). Competent *P. aeruginosa* cells were prepared as described previously (18).

Isolation of ParB mutants impaired in spreading. Plasmid DNA of pKLB2 *tacp-parB* (20 μg) was treated for 20 h with hydroxylamine solution (580 μl of 0.1 M sodium phosphate [pH 6.0], 2 mM EDTA, and 400 μl of hydroxylamine) at 37°C and then dialyzed overnight against TEN buffer (10 mM Tris-HCl [pH 8.0], 1 mM EDTA [pH 8.0], 100 mM NaCl). Mutated DNA was used to transform *E. coli* NR9786 (pABB811). The transformation mixture was plated on selective MacConkey medium with galactose containing streptomycin (selection for resident plasmid), penicillin (selection for incoming plasmid), and 0.5 mM IPTG (ParB overproduction). Transformants forming red colonies were analyzed as carrying pKLB2 with *parB* mutant alleles incapable of transcriptional silencing. Transformants were tested for plasmid integrity and overproduction of ParB forms by Western blotting.

Determination of plasmid compatibility (silencing test). The recipient strain DH5α(pABB811) was transformed with pGBT30 expression vector, pKLB2, and its mutated derivatives. Next, 100 μl of undiluted and serially diluted transformation mixtures was plated in repetition on three different selection plates. The selection was either for incoming plasmid only (L agar with penicillin) for both resident and incoming plasmids (L agar with penicillin and streptomycin), and the double selection plates were supplemented with 0.5 mM IPTG.

Purification of His_6-tailed polypeptides. Exponentially growing BL21(DE3) strains with pET28mod derivatives (36) were induced with 0.5 mM IPTG at a cell density of $\sim 10^8$ cells ml^{-1} and grown for an additional 2 h with shaking at 37°C. The cells were harvested by centrifugation and sonicated. Overproduced His-tagged proteins were purified on Ni-agarose columns with an imidazole gradient in phosphate buffer (pH 8.0) as recommended by the manufacturer (Qiagen) for soluble native proteins. The purification procedure was monitored by SDS-PAGE using a Pharmacia PHAST gel system.

Circular dichroism spectra. Purified His_6-ParB and its derivatives in 100 mM NaF were analyzed at wavelengths between 190 and 260 nm at 20°C by using a JASCO JA-810 spectropolarimeter and quartz cuvettes 0.005, 0.02, and 0.01 cm in depth.

Analytical ultracentrifugation (sedimentation velocity). Sedimentation velocity experiments were carried out in Beckman XL-A analytical ultracentrifuge equipped with absorbance optics. Proteins were diluted in 50 mM sodium phosphate buffer (pH 8.0), 100 mM NaCl, and 1% glycerol to a concentration of 0.1 mg ml^{-1} and centrifuged overnight at 129,000 × *g* at 4°C. Scans at an absorbance wavelength of 280 nm were taken every 6 min. The SEDFIT program was used to analyze 95 scans for each protein, which represents the full extent of sedi-

TABLE 3. Plasmids constructed in this study

Plasmid	Relevant features[a]
pKLB2 derivatives	
pAGB3.3	*tacp-parB* G289→A (A97T)
pAGB3.4	*tacp-parB* C473→T (A158V)
pAGB3.5	*tacp-parB* G656→A/G667→A (R219H/A223T)
pAGB3.6	*tacp-parB* C280→T (R94C)
pAGB3.7	*tacp-parB* G593→A (G198D)
pAGB3.8	*tacp-parB* C748→T (stop249)
pAGB3.9	*tacp-parB* G212→A (G71D)
pAGB3.10	*tacp-parB* C319→T (P107S)
pAGB3.11	*tacp-parB* C290→T (A97V)
pAGB3.12	*tacp-parB* C365→T/Δ758-769 (A122V/Δ253-256)
pAGB3.13	*tacp-parB* G570→A (M190I)
pAGB3.14	*tacp-parB* G140→A (G47D)
pAGB3.15	*tacp-parB* G211→A (G71S)
pAGB3.16	*tacp-parB* C500→T (T167I)
pAGB3.17	*tacp-parB* C494→T (T165I)
pMKB3.18	*tacp-parB* C365→T (A122V)
pMKB3.19	*tacp-parB* Δ758-769 (Δ253-256)
pET28mod derivatives[b]	
pMKB1.3	T7*p-parB* G289→A (A97T)
pMKB1.4	T7*p-parB* C473→T (A158V)
pMKB1.5	T7*p-parB* G656→A/G667→A (R219H/A223T)
pMKB1.6	T7*p-parB* C280→T (R94C)
pMKB1.7	T7*p-parB* G593→A (G198D)
pMKB1.8	T7*p-parB* C748→T (stop249)
pMKB1.9	T7*p-parB* G212→A (G71D)
pMKB1.10	T7*p-parB* C319→T (P107S)
pMKB1.11	T7*p-parB* C290→T (A97V)
pMKB1.12	T7*p-parB* C365→T/Δ758-769 (A122V/Δ253-256)
pMKB1.13	T7*p-parB* G570→A (M190I)
pMKB1.14	T7*p-parB* G140→A (G47D)
pMKB1.15	T7*p-parB* G211→A (G71S)
pMKB1.16	T7*p-parB* C500→T (T167I)
pMKB1.17	T7*p-parB* C494→T (T165I)
pMKB1.18	T7*p-parB* C365→T (A122V)
pMKB1.19	T7*p-parB* Δ758-769 (Δ253-256)
pBBR1MCS1 derivatives[c]	
pMKB2.3	$lacI^q$ *tacp-parB* G289→A (A97T)
pMKB2.4	$lacI^q$ *tacp-parB* C473→T (A158V)
pMKB2.5	$lacI^q$ *tacp-parB* G656→A/G667→A (R219H/A223T)
pMKB2.6	$lacI^q$ *tacp-parB* C280→T (R94C)
pMKB2.7	$lacI^q$ *tacp-parB* G593→A (G198D)
pMKB2.8	$lacI^q$ *tacp-parB* C748→T (stop249)
pMKB2.9	$lacI^q$ *tacp-parB* G212→A (G71D)
pMKB2.10	$lacI^q$ *tacp-parB* C319→T (P107S)
pMKB2.11	$lacI^q$ *tacp-parB* C290→T (A97V)
pMKB2.12	$lacI^q$ *tacp-parB* C365→T/Δ758-769 (A122V/Δ253-256)
pMKB2.13	$lacI^q$ *tacp-parB* G570→A (M190I)
pMKB2.14	$lacI^q$ *tacp-parB* G140→A (G47D)
pMKB2.15	$lacI^q$ *tacp-parB* G211→A (G71S)
pMKB2.16	$lacI^q$ *tacp-parB* C500→T (T167I)
pMKB2.17	$lacI^q$ *tacp-parB* C494→T (T165I)
pMKB2.18	$lacI^q$ *tacp-parB* C365→T (A122V)
pMKB2.19	$lacI^q$ *tacp-parB* Δ758-769 (Δ253-256)
pAKE600 derivatives	
pMKB4	BamHI-SalI fragment of pKLB3 carrying *parA-parB*[d]
pMKB4.3	pMKB4 with *parB* G289→A (A97T) (PCR mutagenesis with primers 5 and 6)*
pMKB4.4	pMKB4 with *parB* C473→T (A158V) (PCR mutagenesis with primers 7 and 8)*
pMKB4.6	pMKB4 with *parB* C280→T (R94C) (PCR mutagenesis with primers 9 and 10)*
pMKB4.15	pMKB4 with *parB* G211→A (G71S) (PCR mutagenesis with primers 11 and 12)*
pMKB4.17	pMKB4 with *parB* C494→T (T165I) (PCR mutagenesis with primers 13 and 14)*

[a] *, The primer sequences are given in Table S1 in the supplemental material.
[b] Plasmid derivatives with EcoRI-SalI fragments with *parB* from relevant pKLB2 derivatives.
[c] Plasmid derivatives with BamHI-SalI fragments with $lacI^q$ *tacp-parB* from relevant pKLB2 derivatives.
[d] The *parA* allele is truncated at the 5′ end.

mentation of the sample. Sedimentation coefficient distributions were calculated by using the Lamm equation modeling implementing maximum entropy regularization (46).

DNA-binding affinity assay. Purified His_6-tagged ParB polypeptides were used in a DNA-binding electrophoretic mobility shift assay (EMSA) as previously described (32). Portions (5.6 pmol) of the double-stranded *parS* oligonucleotide AGCTTGTTGCTTGTTCCACGTGGAACAAGGCCG were incubated with increasing amounts of ParB derivative (10, 20, 30, and 50 pmol) in binding buffer (20 mM Tris-HCl [pH 8.0], 1 mM dithiothreitol, 150 mM NaCl) at 37°C for 15 min. The samples were analyzed on 10% polyacrylamide gels run in 1× Tris-borate-EDTA (TBE) (45). The gels were stained with ethidium bromide, and DNA was visualized in UV light.

Cross-linking with glutaraldehyde. Purified His-tagged ParB derivatives at concentrations either of 0.1 or 0.3 mg ml^{-1} were cross-linked with increasing concentrations of glutaraldehyde (0.0001 to 0.01%) as described previously (20). Protein complexes were separated on SDS-PAGE gels and analyzed by Western blotting with anti-ParB antibodies.

Western blot technique. The cultures of PAO1161 and its mutant derivative strains were grown in L broth to exponential phase. In the "silencing" experiments, the cultures of DH5α carrying pKLB2 derivatives were induced with 0.5 mM IPTG for at least 2 h. Cells were collected, and serial dilutions were plated on L agar to estimate the CFU. Extracts from approximately the same number of cells were separated by SDS-PAGE. Proteins were transferred onto nitrocellulose membranes, and Western blotting with anti-ParB or anti-ParA antibodies was performed as described previously (5).

Introduction of *parB* mutated alleles into the *P. aeruginosa* PAO1161 chromosome by homologous recombination. Competent *E. coli* strain S17-1 was transformed with pAKE600 suicide vector derivatives (11). Overnight cultures of the transformants (donor strains) and the recipient *P. aeruginosa* PAO1161Rif^r were conjugated and integrants treated as described before (30). The allele exchange was verified by PCR using chromosomal DNA as a template and the parB1/parB2 pair of primers. The amplified *parB* orfs were first digested with appropriate restriction enzymes and then sequenced to confirm the presence of derived mutations.

***P. aeruginosa* growth experiments.** $PAO1161_{Rif}$, $PAO1161parB_{null}$, and the various newly constructed PAO1161 *parB* mutant strains were grown overnight and then diluted 1:100 into fresh L broth. Transformants of $PAO1161parB_{null}$ with pBBR1MCS1 vectors containing wild-type (WT) or mutated *parB* alleles were grown on selective medium overnight and diluted in fresh L broth with antibiotic without or with 0.5 mM IPTG for *tac* promoter (*tacp*) induction. The cultures were incubated at 37 or 30°C with vigorous shaking, and the OD_{600} was measured every hour for the first 8 h of growth. Samples were diluted and spread on L agar to estimate CFU.

DAPI staining. Cells were placed on slides covered with 0.01% poly-L-lysine (Sigma). The typical volumes used were 5 μl for a culture in mid-log phase and 1 μl diluted in 4 μl of LB medium for a culture in stationary phase. The bacteria were allowed to adhere to the poly-L-lysine layer for 5 min. Unbound bacteria were washed out by rinsing the slide twice with phosphate-buffered saline (10 mM sodium phosphate [pH 7.4], 15 mM KCl, 150 mM NaCl). Cells were then fixed using 3.7% formaldehyde and stained with DAPI (5 μg ml^{-1}) for 15 min. From this point onward, the slides were kept in the dark. Cells were analyzed by using a Nikon Eclipse EC 800 microscope. Phase-contrast images were collected using Lucia G software, whereas DNA stained with DAPI was visualized using Lucia G/F software. Overlays of images were obtained with the Lucia G/F software (Nikon).

Immunofluorescence microscopy. Portions (10 μl) of affinity-purified anti-ParB antibodies (5) were used as primary antibodies (a 1:100 dilution in 2% [wt/vol] bovine serum albumin [BSA]-PBS), followed by 1 μl of anti-rabbit IgG fluorescein isothiocyanate (FITC)-conjugate solution (6.9 μg ml^{-1} in 2% [wt/vol] BSA/PBS) (Sigma).

Molecular modeling. Atomic coordinates of the ParB three-dimensional monomer model were obtained from the Swiss-MODEL server (2, 49) on the basis of crystallographic data for KorB of RK2/RP4 plasmid (PDB entry 1R71) and Spo0J of *Thermus thermophilus* (PDB entry 1VZ0). The structures of KorB and Spo0J monomers are significantly similar, as shown by the FATCAT server (56) with a *P* value of 2.20e−06, although the predicted "dimer" formation and its interaction with DNA seem to be different for the two proteins. Two models for ParB dimers were created: N-terminal P114-T229 fragments modeled on the basis of the KorB RK2/RP4 structure (26) and N-terminal Q37-L224 fragments modeled on the basis of Spo0J from *T. thermophilus* structure (32). The structures of the WT and mutated ParB proteins were subjected to energy minimization *in vacuo* using an AmberFF99 force field as implemented in Sybyl×1.2 (Tripos, Inc.).

RESULTS

Isolation of *parB* mutants impaired in spreading. It has been shown previously (5) that ParB of *P. aeruginosa*, when in excess, is able to bind to the centromere-like sequence *parS*, spread on DNA, and silence the expression of the genes adjacent to *parS*. The *E. coli* strain DH5α carrying pABB811 (the stably inherited test plasmid based on the pSC101 replicon [9] with *parS* inserted 200 bp from the *repA* promoter [5]) was transformed with the high-copy expression vector pKLB2 *tacp-parB*. The frequency of double transformants selected in the presence of IPTG was 10^5-fold lower than the number of transformants selected only for incoming plasmid. Transformation of the same competent cells with empty vector pGBT30 showed no IPTG effect. Even slight overproduction of WT ParB in *trans* to plasmid with *parS* (uninduced conditions) gave a 10-fold decrease in the number of double transformants compared to DH5α(pABB811) transformed with empty vector pGBT30 (5). When *parS* was absent in the resident plasmid (pGB2), no plasmid loss was observed after transformation with pKLB2 in the presence of IPTG (the same frequency of transformation was observed when selecting either for incoming plasmid or both incoming and resident plasmid). Since the reduction in numbers of double transformants arising in the presence of excess ParB was such a strong phenotype, we applied it to select for *parB* mutants unable to spread and transcriptionally silence the *repA* gene.

Plasmid DNA of pKLB2 mutagenized *in vitro* with hydroxylamine was used to transform *E. coli* NR9786 strain carrying pABB811. The transformants were plated on MacConkey media with galactose containing penicillin, streptomycin, and IPTG to induce ParB production. The *parB* gene in pKLB2 is inserted between the *tac* promoter and the *galK* gene involved in the utilization of galactose as a carbon source. Mutants of pKLB2 impaired in the transcriptional signals could then be easily identified as unable to rescue the galactose fermentation in the recipient strain. Approximately 10% of transformants formed white colonies on MacConkey plates and were excluded from further analysis. The plasmid profiles of 49 putative mutants were also analyzed to eliminate plasmids with visible rearrangements or lowered copy number, but all transformants seemed to carry the plasmids identical to pKLB2 (data not shown). Finally, extracts from exponentially growing cultures of transformants induced by the presence of IPTG were checked by SDS-PAGE, followed by Western blotting with anti-ParB (data not shown). The mutants could be divided into three groups: (i) mutants with no detectable ParB (n = 11), (ii) mutants with visibly truncated ParBs (n = 18), and mutants with ParBs with a molecular mass close to that of WT ParB and produced at levels similar to the WT ParB level (n = 20). DNA sequencing revealed that most of the mutants in the first two groups of *parB* mutants still producing ParB protein had acquired stop codons at different positions and therefore produced truncated ParBs deprived of the C-terminal domain that is responsible for dimerization, which we have shown to be essential for all detectable activities of ParB (J. Mierzejewska, unpublished data). The shortest identified *parB* deletion leading to a "silencing" deficiency removed just seven amino acids from the C terminus. Among the third group of mutants we found a number of single- or double-nucleotide substitutions,

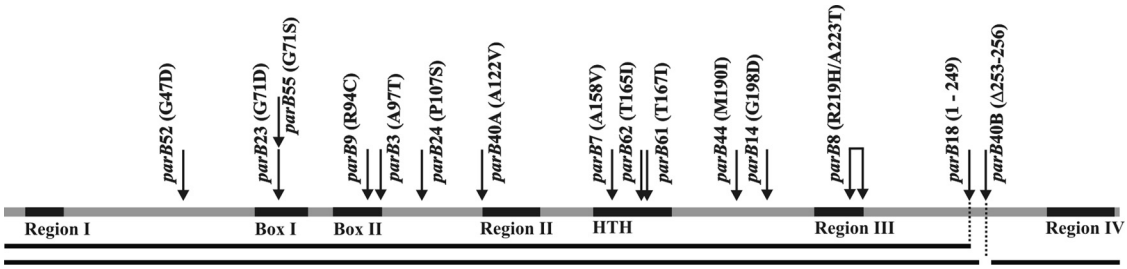

FIG. 1. Summary of "silencing" *parB* mutants of *P. aeruginosa* used in the present study. A schematic map of ParB (290 amino acids) with highly conserved motifs (5) marked in black and the approximate positions of amino acid substitutions in ParB derivatives defective in silencing ability (mutant alleles selected in pKLB2 *tacp-parB*) is shown. The deletion mutants are presented underneath the scheme. The ParB derivative with two regions modified A122V and Δ253-256 was originally encoded by allele *parB40* and was also included in the analysis.

so 12 alleles were chosen for further analysis. One of the alleles, *parB40*, encoded a ParB derivative with a substitution of A122V (in conserved region 2) and an in-frame deletion of four amino acids in the C-terminal domain close to the variable linker region (visible on a Western blot as a slightly truncated ParB version). The individual mutations were introduced by site-directed mutagenesis and, for further analysis, we used the double mutant producing ParB A122V/Δ253-256 and single mutants producing ParB A122V and ParB Δ253-256 separately (Fig. 1). The mutant allele *parB14* producing ParB without the C-terminal 51 amino acids was also included in the analysis as an internal control representing protein definitely unable to dimerize.

The mutated plasmids were introduced again into strain DH5α (pABB811) to confirm the deficiency in silencing of the *repA* promoter. Transformants were plated out with selection for the incoming plasmid, for both incoming and resident plasmids and with selection for both plasmids in the presence of IPTG. We observed, after induction with IPTG, a 10^5-fold decrease in the number of transformants for WT ParB (pKLB2) but no difference in the frequency of transformations for any of the mutants except *parB40A* (see Fig. S1 in the supplemental material). The overproduction of ParB A122V gave a strong silencing effect comparable to that of WT ParB, whereas ParB Δ253-256 was impaired in the ability to silence the *repA* gene. Further functional analysis indicated no differences between ParB A122V/Δ253-256 and ParB Δ253-256, so for clarity only results for the deletion mutant producing ParB Δ253-256 are presented. Western blot analysis with anti-ParB antibodies of extracts from transformants grown in the presence of IPTG showed neither significant differences in the level of ParB overproduction between WT ParB and mutant derivatives nor increased instability of mutant versions of ParB (data not shown).

The N terminus of ParB is involved in oligomerization. The *parB* mutant alleles were recloned into pET28mod vector and their products were purified as N-terminally His_6-tagged derivatives. Purified ParB mutant derivatives were initially screened by circular dichroism (CD) measurements at wavelengths between 190 and 260 nm to check for major perturbations in protein structure. Analysis of CD spectra revealed no significant changes in the α-helical content in the secondary structure of any of the tested proteins in comparison to WT ParB (even the shorter form of ParB 1-249); hence, only CD spectra for representative ParB derivatives are shown in Fig. 2. The ability of ParB derivatives impaired in spreading to form high-molecular-mass structures was tested by two methods: analytical ultracentrifugation and cross-linking with glutaraldehyde. The results from analytical ultracentrifugation (Fig. 3A) demonstrated that WT ParB exists mainly as dimers in solution, and no higher-order complexes (e.g., tetramers) were detected. The results also showed that all ParB spreading mutants were still able to dimerize (data are presented for only two representative derivatives, ParB T167I and ParB M190I). On the other hand, ParB 1-249 remained monomeric, whereas the short deletion derivative ParB Δ253-256 seemed to form less-stable dimers than other tested proteins.

Cross-linking with glutaraldehyde and separation of complexes by SDS-PAGE confirmed the ability of 10 derivatives to form dimers (molecular mass of ~66 kDa) with the exception of ParB 1-249, ParB G71S, ParB G71D, and ParB Δ253-256, for which dimers could not be observed by this method (see Fig. S2 in the supplemental material). To better visualize the higher-molecular-mass forms, cross-linked proteins were sep-

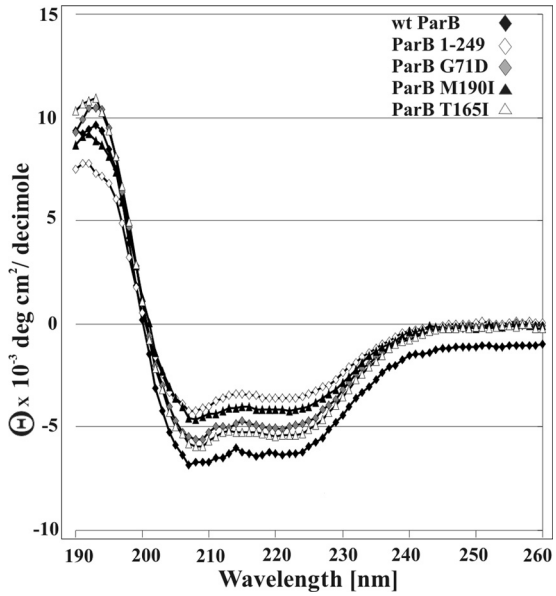

FIG. 2. Circular dichroism spectra of ParB derivatives. Purified 6×His-tagged versions of mutated ParB were analyzed by CD as described in Materials and Methods. Since all spectra were similar, only four are shown as representative ParB derivatives for clarity.

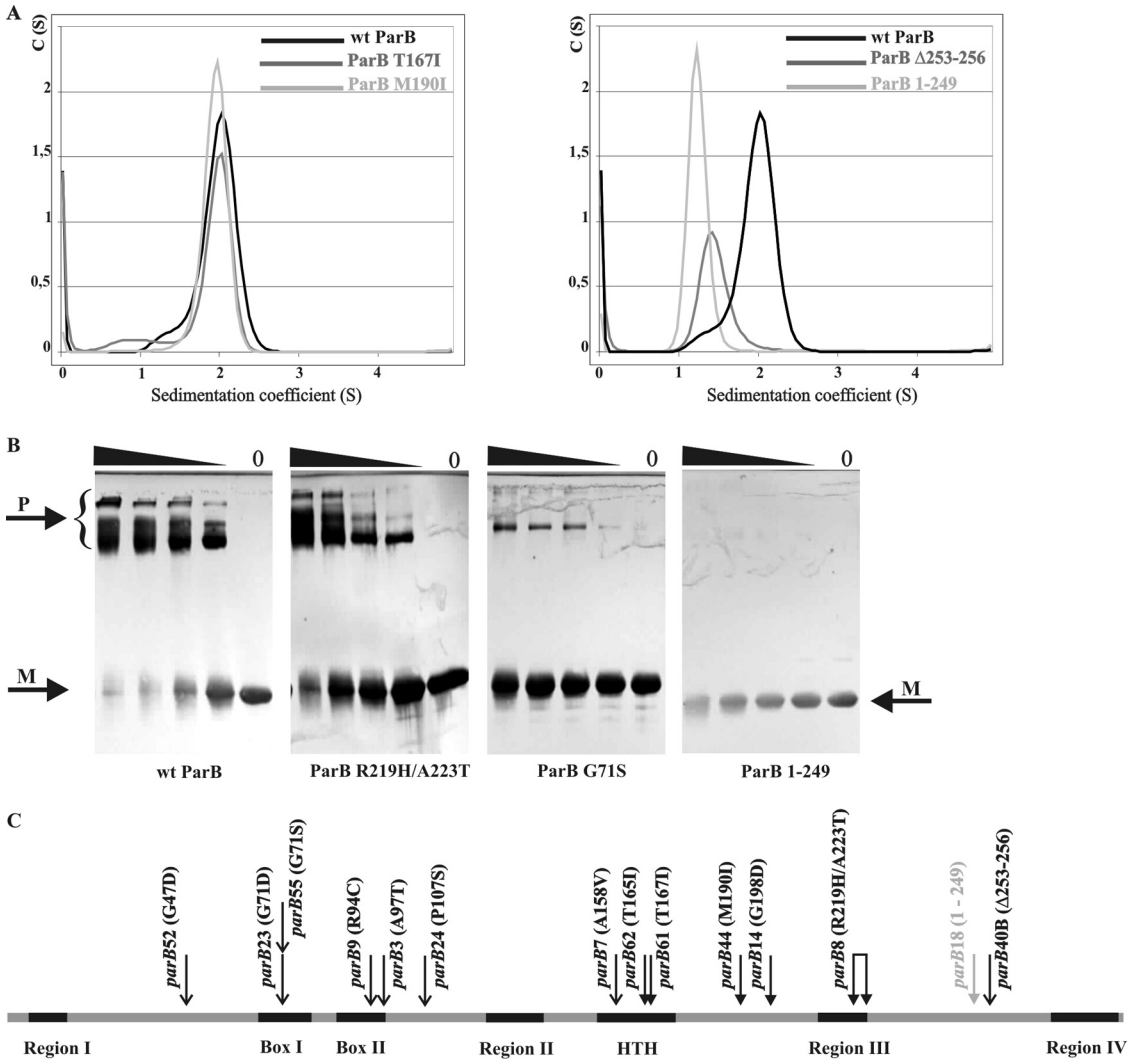

FIG. 3. Structural analysis of ParB derivatives. (A) Analytical ultracentrifugation of ParB derivatives. Purified His_6-tagged versions of mutated ParB at concentrations 0.1 mg ml^{-1} were centrifuged in the Beckman XL-A ultracentrifuge in sets of eight tubes, with WT ParB and ParB 1-249 included in each set. "S" represents the sedimentation coefficient. Comparison of the S values for four ParB mutants are shown, where an S value close to 2 corresponds to dimeric form of the protein and an S value close to 1 corresponds to the monomeric form of the protein. (B) Cross-linking of ParB derivatives with glutaraldehyde (GA). Purified His_6-tagged proteins at 0.3 mg ml^{-1} were incubated at room temperature for 20 min (18) without or with different concentrations of glutaraldehyde: 0.001, 0.002, 0.005, and 0.01%. Proteins were separated by SDS-PAGE on 12% gels and visualized by Western blotting with anti-ParB antibodies. Monomers are indicated as "M," and higher-order are indicated as complexes as "P." (C) Graphic summary of the ability of ParB mutants to form higher-order complexes. Localization of analyzed mutations is indicated by arrows. Black solid arrows indicate mutants with the ability to form higher-order complexes comparable to WT ParB. Black V-type arrows indicate mutants impaired in higher-order complex formation. The gray arrow indicates mutant ParB 1-249, which remains in the monomeric state.

arated by SDS-PAGE, transferred to nitrocellulose filters, and analyzed by Western blotting with anti-ParB antibodies. We used two different concentrations of proteins (0.1 and 0.3 mg/ml, respectively) and treated the proteins with glutaraldehyde in the presence or absence of double-stranded oligonucleotide corresponding to *parS*. The ability to be cross-linked did not depend on the presence of DNA for any of the analyzed proteins. Only ParB 1-249 remained strictly monomeric under all conditions. Other ParB proteins were able to form higher-order complexes, although some of them with less efficiency than WT ParB at the same concentration of protein and cross-linking agent (Fig. 3B). The results for all tested ParB derivatives are shown in Fig. S3 in the supplemental material. On the basis of the ability to form higher-order structures, the proteins were separated into two groups. ParB derivatives G47D, G71S(D), R94C, A97T, P107S, and A158V were all noticeably impaired in oligomerization ability under these conditions. The ParB T165I, T167I, M190I, and G198D mutants and the double mutant R219H/A223T showed no defect in the *in vitro* oligomerization test. The results from analytical ultracentrifugation and cross-linking experiments are summarized in Fig. 3C and Table 4. The results indicated that while the C-terminal dimerization domain is the major determinant of higher-order complex for-

TABLE 4. Summary of analysis of *parB* mutants

No. of *parB* allele (substitution) conserved motif[a]	Form in the solution (AUC)	Higher-order complex formation (after GA cross-linking)	DNA binding (EMSA)	Toxic effect (after overproduction in PAO1161*parB*)
Wild type	Dimer	+++	+++	+++
52 (G47D)	Dimer	+	+++	+
23 (G71D) Box I	Dimer	+	+	+
55 (G71S)*, Box I	Dimer	+	+	+
9 (R94C), Box II	Dimer	+	+++	+
3 (A97T), Box II	Dimer	+	+++	+++
24 (P107S)	Dimer	+	+++	−
7 (A158V), H-T-H	Dimer	+	+++	+
62 (T165I), H-T-H	Dimer	+++	−	+
61 (T167I), H-T-H	Dimer	+++	−	−
44 (M190I)	Dimer	+++	+	+
14 (G198D)	Dimer	+++	−	+
89 (R219H/A223T), region III	Dimer	+++	−	+
40B (Δ253-256)	Dimer/monomer	+	+	+
18 (stop249)	Monomer	−	−	+

[a] *, The *parB* alleles introduced into PAO1161 chromosome by allele exchange are shaded.

mation, several residues in the N-terminal of ParB play an important role in oligomerization.

The H-T-H motif of ParB is required but not sufficient for effective DNA recognition/binding. EMSAs using mutated ParB proteins were performed to check the ability of these proteins to bind double-stranded oligonucleotides corresponding to the $parS_2$ sequence. It was previously demonstrated that WT ParB exhibits the highest affinity to this perfect palindrome sequence among tested *parS* sites (5). The His_6-tagged WT ParB was used as a positive control, whereas an unrelated double-stranded oligonucleotide served as the negative control (nonspecific binding [data not shown]). DNA-protein complexes were separated by PAGE. The group of ParB mutants unable to bind *parS* oligonucleotide consisted of ParB T165I, T167I, and G198D; the double-mutant ParB R219H/A223T; and ParB 1-249 with the C terminus removed (see Fig. S4 in

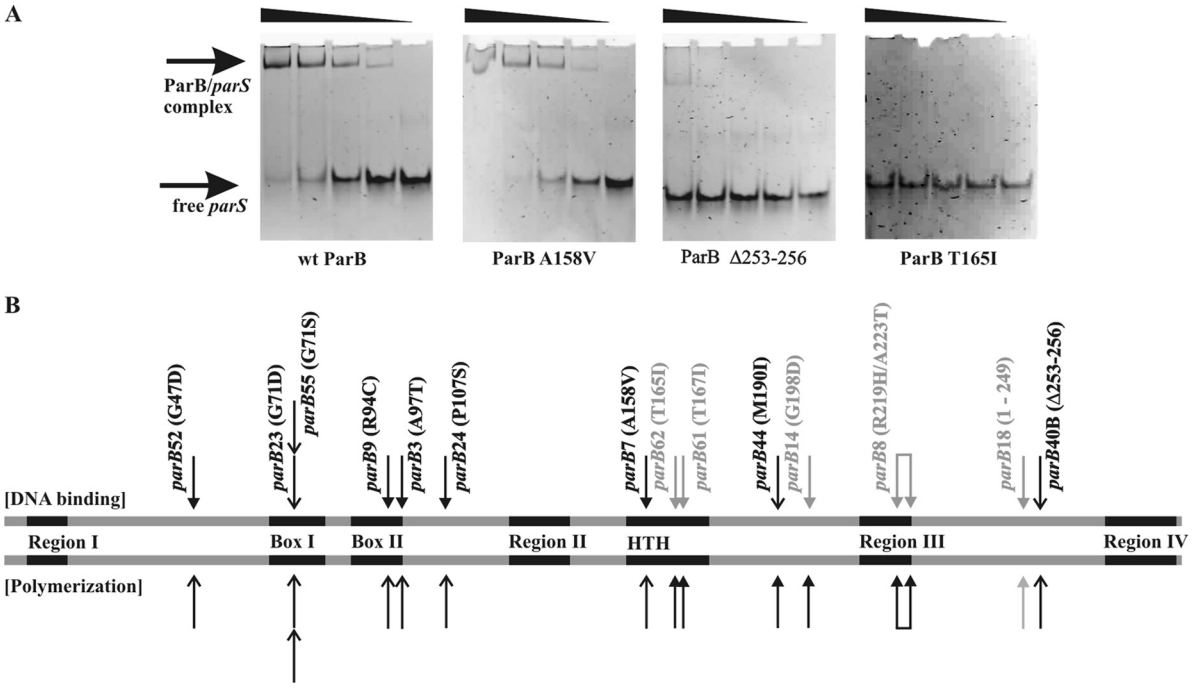

FIG. 4. DNA-binding activity of ParB derivatives. (A) EMSA for representative ParB derivatives. Different amounts (10, 20, 30, and 50 pmol) of purified ParB proteins were incubated with 5.6 pmol of *parS* double-stranded oligonucleotide at 37°C for 15 min. The samples were analyzed on 10% (wt/vol) nondenaturing polyacrylamide gels run in TBE. After electrophoresis, the gels were stained with ethidium bromide, DNA was visualized in UV light and photographed. (B) Graphic summary of DNA-binding affinity of ParB mutants. Localization of analyzed mutations is indicated by arrows. Three types of arrow correspond to distinct DNA binding abilities: highly impaired mutants are indicated by gray arrows, partially impaired mutants are indicated by black V-type arrows, and mutants binding to DNA with WT ParB activity are indicated by black solid arrows. For comparison, the results for oligomerization ability of mutant derivatives are shown below the ParB scheme.

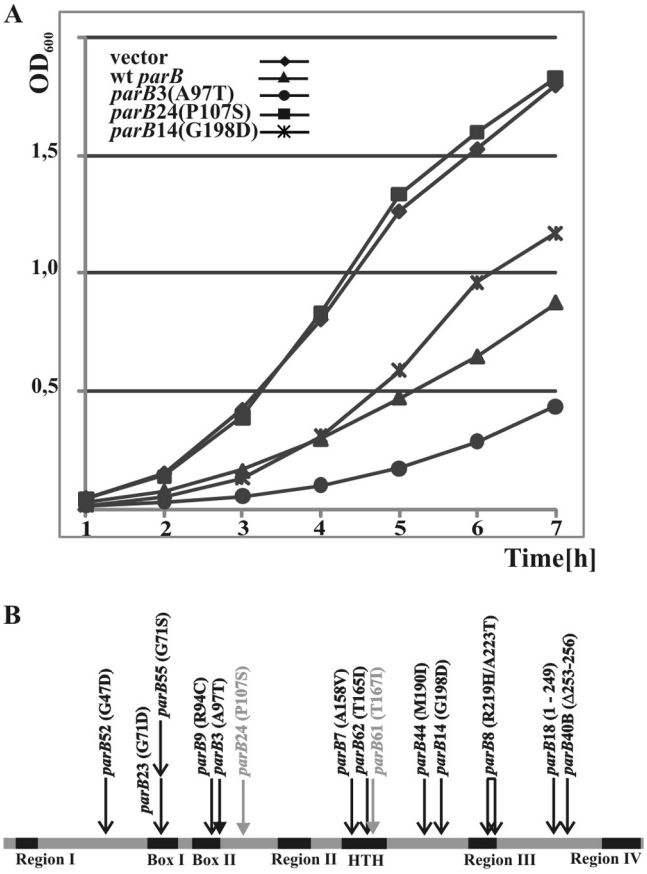

FIG. 5. Growth inhibition of *P. aeruginosa parB*-null mutant by overproduction of ParB mutant derivatives. (A) Growth of PAO1161$parB_{null}$ (pBBR1MCS1 *tacp-parB* mutants). Overnight cultures were diluted 100-fold into L broth supplemented with chloramphenicol or chloramphenicol and 0.5 mM IPTG. The cultures were incubated with shaking at 37°C, and the OD_{600} was measured at hourly intervals. As controls, PAO1161$parB_{null}$(pBBR1MCS1) (vector) and PAO1161$parB_{null}$ (pJMB500) (WT *parB*) were used. For clarity, only the results for IPTG-induced cultures for three representative mutant ParB derivatives are shown. (B) Graphic summary of inhibition effect of ParB derivatives on PAO1161$parB_{null}$ growth. The ParB derivatives retaining a growth inhibition effect when overproduced are indicated either by black solid arrows (high toxicity) or black V-type arrows (slightly lower toxicity), whereas modifications abolishing growth inhibition are indicated by gray solid arrows.

the supplemental material). The remaining proteins were still able to bind *parS* either with affinity comparable to that of WT ParB (ParB G47D, R94C, A97T, P107S, and A158V) or with lower affinity, as observed for ParB G71D, G71S, M190I, and Δ253-256. Figure 4 shows representative data and a summary of the EMSA experiments, whereas data for all ParB mutants tested using EMSA with $parS_2$ are presented in Fig. S4 in the supplemental material. Our previous studies showed that ParB binds to *parS* as a dimer and that a ParB derivative with the H-T-H motif deleted had lost its DNA-binding activity (5). We expected substitutions in the H-T-H motif (ParB A158V, T165I, and T167I) and ParBs with impaired C-terminal dimerization domain (ParB 1-249 and Δ253-256) to be defective in DNA binding, and this was confirmed except for ParB A158V. Two mutants with amino acid substitutions in the sequence following the H-T-H motif (ParB G198D [between region 3 and the H-T-H motif] and ParB R219H/A223T [region 3]) did not bind *parS*. In addition, mutant ParB M190I, also located between region 3 and the H-T-H motif, had a lower binding affinity for *parS*. Since the ability to dimerize and polymerize is not impaired in these derivatives, the new determinants involved in the ParB interactions with DNA have been identified. Two derivatives—ParB G71S and ParB G71D—had lower binding affinities toward *parS*, while substitutions of glycine at position 71 in the highly conserved Box I sequence led to a strong polymerization defect (Fig. 4B).

Deficiency in spreading on the DNA is not equivalent to the loss of ParB toxicity. As shown previously, ParB, when in excess, is able to inhibit the growth of *P. aeruginosa* (5), and this effect is independent of ParA (an excess of ParB is toxic in a *parA*-null mutant) (30). To test the effect of the overproduction of the mutant versions of ParB on *P. aeruginosa*, the alleles were cloned into broad-host-range vector pBBR1MCS1 under the control of the *tacp*. All pBBR1MCS1 derivatives were transformed into a PAO1161 *parB* deletion strain. The cultures of transformants were grown with or without IPTG. The average growth rate in exponential phase was calculated from three independent experiments, while the strains with the empty vector pBBR1MCS1 and pJMB500 were used as controls. The results showed that the overproduction of ParB derivatives impaired in spreading still demonstrated either a very strong toxic effect (ParB A97T), a weaker but significant toxic effect (ParB G47D, G71D, G71S, R94C, A158V, T165I, M190I, G198D, and R219H/A223T; ParB 1-249; and ParB Δ253-256), or no effect (ParB P107S and T167I). DNA binding and spreading is therefore not the main factor responsible for slowing down the growth rate of *P. aeruginosa* in the presence of a ParB excess since some spreading-deficient mutants retained their toxicity (Fig. 5).

ParBs defective in spreading cause defects in chromosome segregation and changes in cell motilities. To analyze the role of ParB spreading in various cellular functions, five *parB* alleles—*parB55*, *parB9*, *parB3*, *parB7*, and *parB62* (coding for ParB G71S, R94C, A97T, A158V, and T165I, respectively)—were introduced into the PAO1161 chromosome. The products

TABLE 5. Growth rate and percentage of anucleate cells formation for *P. aeruginosa* WT and *parB* mutants

P. aeruginosa strain[a]	Division time (min) at 30°C on L broth[b]	% Anucleate cells in population[c]
PAO1161	42	<0.03
PAO1161$parB_{null}$	54	2.30
PAO1161$parB_{55}$ (G71S)	44	1.41
PAO1161$parB_{9}$ (R94C)	45	1.31
PAO1161$parB_{3}$ (A97T)	44	2.3
PAO1161$parB_{7}$ (A158V)	41	1.2
PAO1161$parB_{62}$ (T165I)	55	2.4

[a] The amino acid substitution in the ParB derivative is indicated in parentheses.

[b] Cultures were grown at 30° on L broth and at hourly intervals appropriate dilutions were spread on L-agar plates to estimate the CFU. The division time was calculated from three independent cultures.

[c] Cells from a logarithmically grown culture were DAPI stained and visualized by microscopy. The percentage of anucleate cells was estimated in three experiments on the sample of at least 1,000 cells each.

of the mutated alleles when analyzed *in vitro* differed in their ability to bind DNA, form higher-order complexes, and disturb cell growth or divisions when overproduced (Table 4). The mutant alleles were cloned into the suicide vector pAKE600 (11) and then introduced into the *P. aeruginosa* genome by homologous recombination. The allele exchange was confirmed by sequencing of *parB* genes amplified by PCR on chromosomal DNA of the putative mutants. Separation of proteins from mutant strains by SDS-PAGE and analysis by Western blotting confirmed that the level of ParB production was comparable to that of WT strain PAO1161 (see Fig. S5 in the supplemental material). The extracts were also screened for the presence of ParA with anti-ParA antibodies and showed no differences in the level of ParA production between PAO1161 and the various *parB* mutants (data not shown).

Chromosomal mutants were tested for growth rate and colony morphology, two types of motility (swimming and swarming), cell size, chromosome segregation, anucleate cell production (by DAPI staining), and ParB focus formation (by immunofluorescence microscopy using primary anti-ParB antibodies and FITC-conjugated secondary antibodies). The colony morphology of tested mutants was indistinguishable from the *parB*-null mutant: they formed irregular-shaped colonies in contrast to the smooth-edged colonies of the WT strain (data not shown). Growth rate was much slower in mutant PAO1161$parB_{62}$ (comparable to strain PAO1161$parB_{\text{null}}$), whereas in four other strains the cell division rate was not significantly different from the WT strain (Table 5). All five mutants showed defects in chromosome segregation. The percentage of anucleate cell production by mutants varied between 1.2 and 2.4%, whereas it was <0.03% for the PAO1161 WT and 2.3% for the PAO1161$parB_{\text{null}}$ strains under the same growth conditions (Table 5). The number of anucleate cells was estimated in three independent experiments on the samples of 1,000 cells. Monitoring of ParB localization using the FITC technique showed multiple, randomly distributed, and fuzzy ParB foci in all five mutants (Fig. 6A). Thus, it appears that formation of two to four condensed and regularly spaced foci observed in the WT strain depends on the ability of ParB to bind to DNA and spread. All mutants also showed defects in swarming and swimming, although two of the five mutant strains, PAO1161$parB_7$ (expressing ParB A158V) and PAO1161$parB_{55}$ (expressing ParB G71S), were significantly less impaired than the *parB*-null mutant (Fig. 6B).

DISCUSSION

Representatives of the ParB family (including chromosomal ParBs) have a main dimerization domain located in the C terminus and centrally located H-T-H motif involved in DNA binding (Fig. 7). Conserved N and C domains of ParB protein are separated by a variable linker region (5, 6, 35). The ability to form dimers is a prerequisite for strong operator binding since monomers either do not bind DNA or bind weakly (5, 21, 32). Despite the homology and overall very similar structure ParBs seem to differ significantly in their interactions with DNA. The "transcriptional silencing" function observed for several representatives of the type IA ParB family depends on the ability of the protein to recognize and bind specific DNA sequences (centromere-like *parS*), oligomerize by protein-protein interactions, and spread on DNA starting from *parS* (5, 35, 37). In the present study we analyzed mutant *parB* alleles from *P. aeruginosa* defective in spreading on DNA.

The mutations affecting spreading of ParB from *P. aeruginosa* were found dispersed throughout the protein. The most common *parB* mutants had stop codons producing a range of truncated derivatives, all deprived of the dimerization domain. The shortest deletion from the C terminus, which abolished spreading, had seven amino acids removed, confirming our previous observation about the importance of the C terminus of the ParB protein in dimerization (5). Among the mutants there was also a *parB* allele with a 12-nucleotide deletion in the linker proximal part of the C-domain (in-phase deletion of four amino acids). ParB Δ253-256 was impaired significantly in the dimerization, demonstrating that other residues in region 4 (5) are also involved in self-association.

The residues from the N-terminal part of the protein form the oligomerization surface in ParB. In the present study, we isolated 12 *parB* point mutants impaired in spreading but not in dimerization, a finding previously demonstrated by analytical ultracentrifugation and cross-linking experiments (Fig. 3 and Table 4). None of the ParB derivatives seemed to have a greatly disturbed CD spectrum, suggesting no major misfolding of the proteins. The ParB derivatives mutated in the N terminus—G47D, G71S/D, R94C, A97T, P107S, and A158V—were impaired in the ability to form higher-order complexes, identifying the N-terminal half of ParB as the major oligomerization determinant (Table 4).

Identification of new DNA-binding determinants in the ParB sequence outside of the H-T-H motif. Three of the ParBs with substitutions in the predicted H-T-H motif (Fig. 1) were thought to be impaired in DNA binding, but only two of them, ParB T165I and T167I, with mutations in the recognition helix, were unable to bind *parS*. Among other ParB derivatives defective in *parS* binding were ParB M190I, ParB G198D, and the double-mutant ParB R219H/A223T. These three derivatives with amino acids substitutions localized outside of the H-T-H motif showed no defect in dimerization or oligomerization *in vitro*, suggesting that their inability to spread may be the result of changes in amino acids involved in specific DNA contacts.

Model of ParB-DNA complex formation. For years the attempts to crystallize the intact ParB proteins of type IA from different sources have been unsuccessful. The first structure solved was that of the C terminus of KorB (residues 297 to 358) from RK2 plasmid of IncP-1 (10), representing the dimerization domain. It was followed by crystal structures of part of the N terminus of KorB (residues 117 to 294) crystallized with the O_B KorB binding site (26), the N-terminal residues 1 to 222 of Spo0J (269 amino acids) from *Thermus thermophilus* (32), and fragment from residues 142 to 333 bound to *parS* of ParB of P1 (333 amino acids in total) (47). In a recent report (48), crystals of full-length SopB of the F plasmid (323 amino acids) mixed 1:1 with 18-mer (the *sopC* consensus site) were obtained and resolved; however, the density was only observed for central residues 157 to 271 containing determinants for specific binding to DNA.

ParB from *P. aeruginosa* shares much greater similarity to KorB from the RK2/RP4 plasmid and Spo0J (ParB) from *T. thermophilus* (17 and 36% sequence identities, respectively,

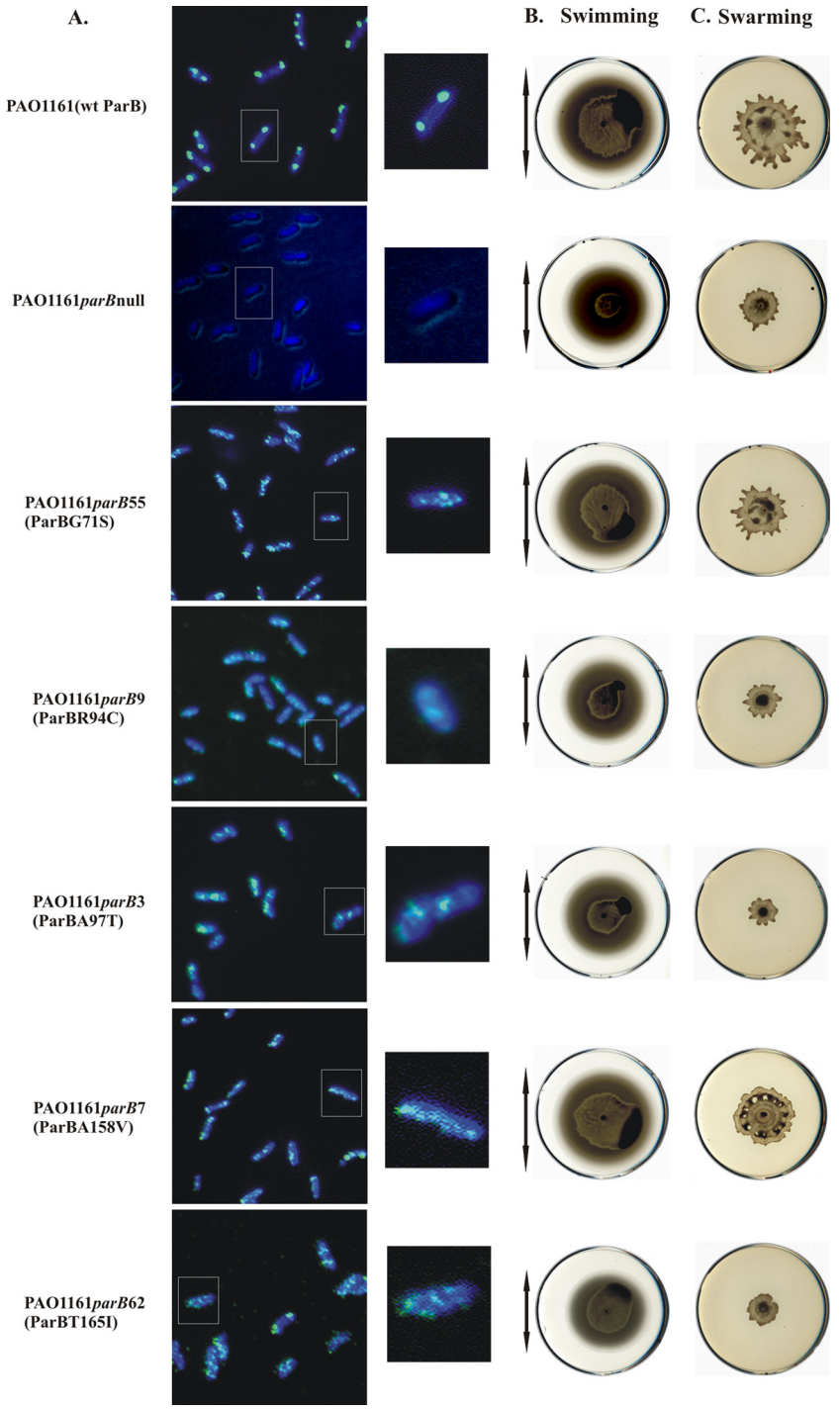

FIG. 6. Characterization of PAO1161 *parB* mutants defective in spreading. (A) ParB subcellular localization in PAO1161 *parB* spreading mutants. Fixed cells were prepared from exponential phase of culture growth (OD_{600} = 0.4) on L broth at 37°C. Overlaid images of immunofluorescence (green) signal and DAPI (blue) staining show ParB foci in the cells of PAO1161 (WT ParB), PAO1161$parB_3$ (ParB A97T), PAO1161$parB_7$ (ParB A158V), PAO1161$parB_9$ (ParB R94C), PAO1161$parB_{55}$ (ParB G71S), and PAO1161$parB_{62}$ (ParB T165I) mutants. Magnifications of single cells are shown for clarity. (B) Swimming motility of PAO1161 *parB* mutants defective in spreading. Arrows demonstrate the diameters of the zones of swimming (extending beyond visible growth zones on the surface). (C) Swarming motility of PAO1161 *parB* mutants defective in spreading.

Fig. 7) than to ParB of P1 plasmid and SopB of F plasmid (47, 48). From the available crystallographic data, two models for $ParB_{Pa}$ have been created on the basis of KorB RK2/RP4 structure (Fig. 8A and B) and Spo0J from *T. thermophilus* (Fig. 8C and D), and mutations defective in either DNA binding or oligomerization were localized in the structure. Neither of these models fully accommodates all of our experimental data. *P. aeruginosa* ParB seems to interact with DNA similarly to

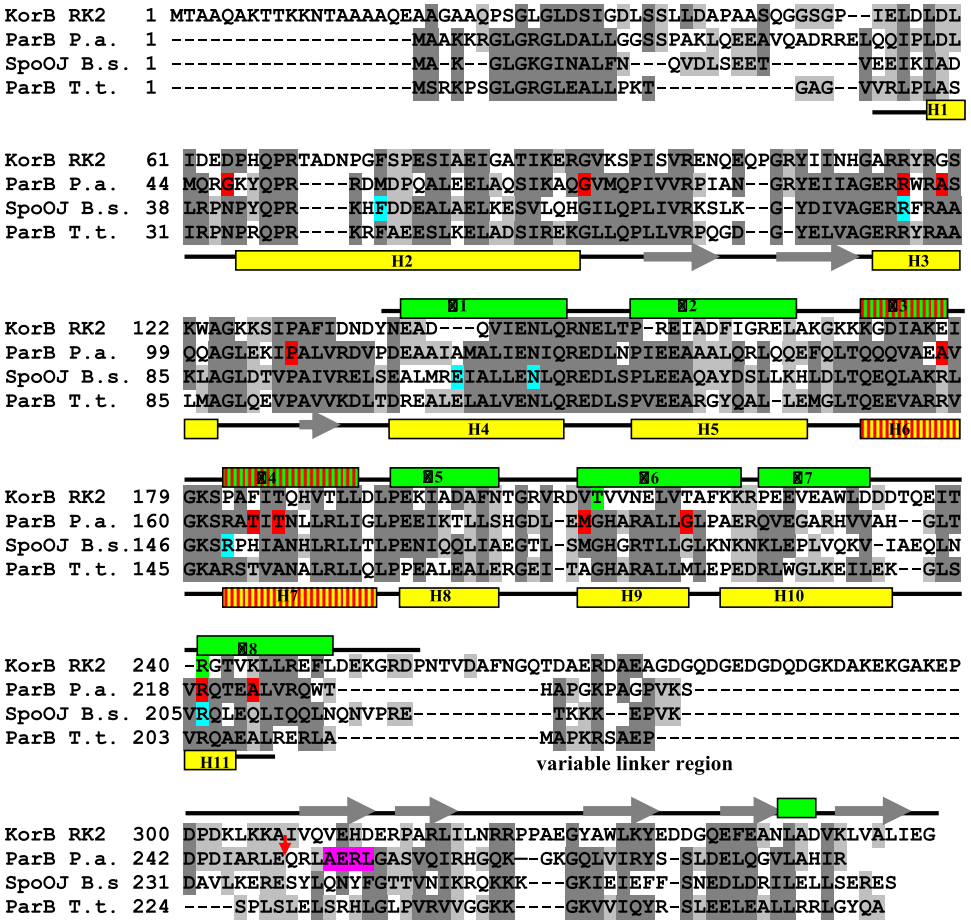

FIG. 7. Alignment of ParB from *P. aeruginosa* PAO1 with selected representatives of ParB family. Dark gray shadowing indicates the similar residues in more than three representatives. Light gray shadowing indicates similarities between two proteins. Structural motifs from crystallographic studies on KorB of plasmid RP4/RK2 (above the alignment in green) and Spo0J/ParB from *T. thermophilus* (indicated below in yellow) are drawn with rectangles corresponding to α-helices and arrows corresponding to β-sheets. Labeling of the helices corresponds to the original nomenclature (26, 32). H-T-H motifs are striped. Red-shaded residues in ParB *P. aeruginosa* sequence correspond to substituted residues, and pink-shaded residues correspond to deleted residues in the course of this study. A red arrow indicates the localization of stop codon in the ParB 1-249 derivative. Green residues marked in the KorB sequence correspond to DNA-binding determinants outside of the H-T-H sequence (26). Blue residues in Spo0J of *B. subtilis* correspond to mutations analyzed previously (3).

KorB, engulfing DNA sequence and not "sitting" on it as the Spo0J model predicts (32). The polymerization deficient mutations in the N terminus of $ParB_{Pa}$ fit into Spo0J *T. thermophilus* structure (the adequate part of KorB has not been crystallized [26]), however, on the assumption that the "dimerization" surface described by the authors (32) is indeed an oligomerization surface (see below).

ParB interacts with DNA in a similar way to KorB. Previous reports on the KorB structure of the RK2/RP4 plasmid (26) demonstrated that four helices make contact with the operator: helices α3 and α4 forming the typical H-T-H motif and also helices α6 and α8 (Fig. 7). While α4 (the recognition helix) plays a role in nonspecific KorB operator binding, it does not contribute to operator sequence recognition. The recognition specificity is based mainly on the two side-chain interactions (hydrogen bonding) outside the H-T-H motif, T211 in α6 and R240 in α8, which was confirmed experimentally by mutagenesis (26). Alignment of the amino acid sequences of KorB and $ParB_{Pa}$ indicated that M190 and G198 of $ParB_{Pa}$ are located in the predicted α6 helix for *P. aeruginosa* ParB (based on the KorB structure; Fig. 7 and Fig. 8A), whereas R219H corresponds to R240 in the KorB structure. On the basis of our mutant analysis, we conclude that the specific DNA binding of $ParB_{Pa}$ outside of H-T-H is highly similar to KorB-DNA interactions, with the exception that the recognition helix of H-T-H (mutant substitutions in T165 and T167 of ParB) is also involved in the specific recognition of *parS*. Computational modeling of the WT and mutated protein structures indicated that A158 of the "stabilization" helix of H-T-H motif is not buried in the DNA duplex and, hence, the substitution A158T may not affect the interactions with DNA (data not shown).

The ParB domain responsible for polymerization corresponds to the Spo0J putative dimerization surface. Only N-terminal domains of KorB and Spo0J proteins were crystallized, both deprived of the main C-terminal dimerization domains. In the biochemical tests (gel filtration, *in vitro* cross-linking, and analytical ultracentrifugation), both truncated proteins were monomeric in solution (26, 32). The fragment of

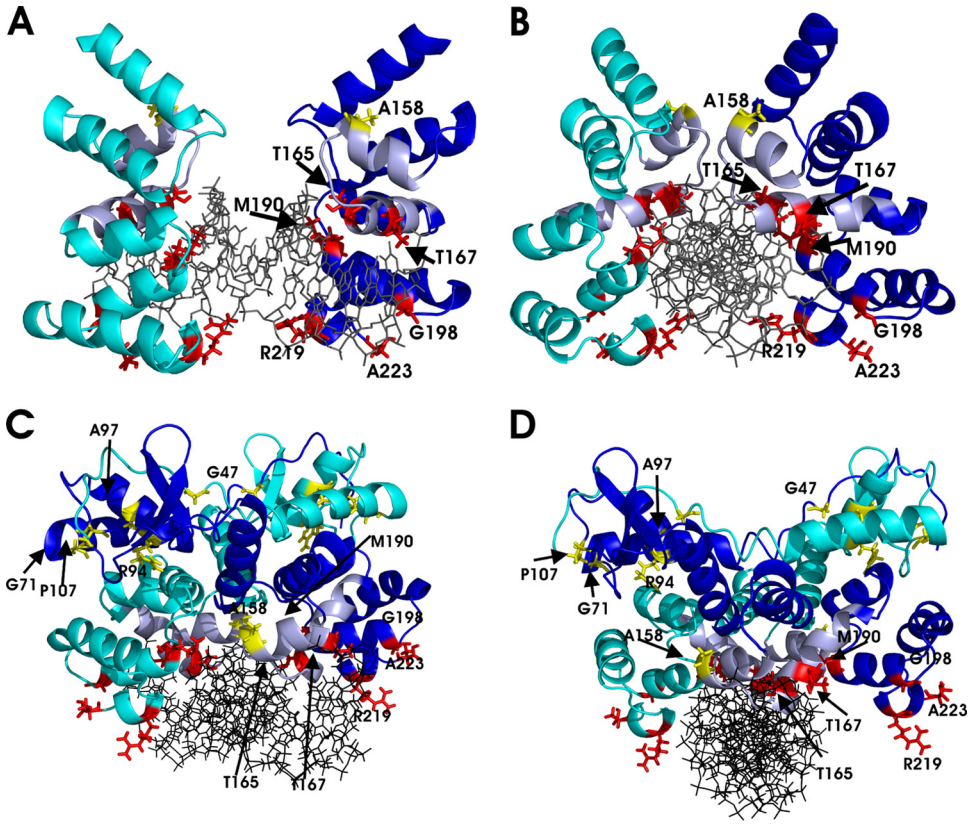

FIG. 8. Model of N-terminal part of ParB from *P. aeruginosa* interacting with DNA. (A and B) Different projections of two ParB monomers (the N-terminal P114-T229 fragment) modeled on the basis of the KorB RK2/RP4 structure (26). (C and D) Different projections of two ParB monomers (the N-terminal Q37-L224 fragment) modeled on the basis of Spo0J from the *T. thermophilus* structure (32). Monomer subunits are indicated in green and dark blue, with regions of the H-T-H highlighted in light blue. Residues mutated in the present study are colored red (impaired in DNA binding) and yellow (impaired in polymerization) in both monomers but numbered only in the dark blue one.

KorB-O was crystallized in the presence of the O_B operator, and binding to DNA linked two monomers in such a way that the operator was completely engulfed within the "dimer" (26). In the case of *T. thermophilus* Spo0J, no DNA was present during crystallization, but the authors still obtained N domains interlinked into antiparallel "dimer" with an extensive dimer interface (28% of the surface of one monomer) (32).

Mutants of $ParB_{Pa}$, which were able to dimerize but not to polymerize, have been found at positions G47 and G71, flanking α-helix H2; at positions R94 and A97 located in α-helix H3; and at P107 preceding the β-sheet S3. This region corresponds to the Spo0J dimer interaction interface (according to the Spo0J model; Fig. 7 and Fig. 8A and B). The glycine at position G71 seems to be particularly important, since two spreading-defective mutants were isolated with substitutions G71S and G71D, respectively. Computational modeling showed no drastic change in folding of mutant proteins (data not shown), although both mutated proteins at position G71 are defective in DNA binding and polymerization, suggesting that amino acid substitutions change flexibility of the protein and diminish its ability for stable self-interactions and interactions with DNA.

Observed "toxicity" of ParB when overproduced is not the result of ParB spreading. All tested mutant ParBs defective in spreading (with the exception of ParB P107S and ParB T167I) inhibit the growth of *P. aeruginosa* when in excess (Fig. 5). However, one of the substitutions (A97T) increased the "toxicity" compared to WT ParB. Computational modeling demonstrated that this substitution introduces structural changes in the region from E61 to L103 (see Fig. S6 in the supplemental material). Our current hypothesis about "toxicity" is that when in excess ParB interacts and sequesters important cell components and interferes with their normal function. It is then feasible that observed changes in ParB A97T modify the protein-protein interaction surface.

Spreading is necessary for ParB's role in cell division and precise nucleoid segregation. The pleiotropic character of *parB* deletion mutants (4) prompted us to introduce five different *parB* alleles with single amino acid substitutions into the PAO1161 chromosome. The growth rate of the four tested *parB* point mutants did not differ from the growth rate of the WT strain, whereas the PAO1161$parB_{62}$ mutant (producing ParB T165I, impaired in DNA binding) had a division time similar to the *parB* deletion mutant. All *parB* substitution mutants were impaired in swarming and swimming (two of three tested motilities), as observed previously for the *parB*-null mutant (4); however, the deficiency in motilities was less pronounced in the presence of ParB A158V and ParB G71S. At present, we cannot explain these differences between particular mutant derivatives. Despite the fact that mutated ParBs

were defective either in DNA binding (ParB T165I), oligomerization (ParB A97T, R94C, and A158V) or both (ParB G71S), all of them demonstrated aberrant chromosome segregation and formed from 1.2 to 2.4% anucleate cells under logarithmic growth conditions. Delocalized, multiple, and fuzzy ParB foci were also observed in all five mutants (Fig. 6). Since the common feature of the tested mutant ParB proteins was the inability to spread on DNA, we can conclude that any mutation prohibiting spreading yields a phenotype similar to the lack of ParB in relation to the chromosome segregation and the ability to move.

The only previous mutant analysis of chromosomal homologue of ParB family was performed on Spo0J from *B. subtilis* (3). Among sporulation-deficient *spo0J* mutants, amino acid substitution R206C was found at a position corresponding to our mutant ParB R219H deficient in spreading (Fig. 7). The R206C substitution in Spo0J leads to an abnormal nucleoid appearance, dispersed Spo0J foci, and loss of DNA binding similarly to ParB R219H. Another *spo0J* mutant (*spo0J13*) impaired in focus production and chromosome segregation produced Spo0J R80A corresponding in position to our mutant ParB R94C (Fig. 7). Both of these mutations in ParB and Spo0J do not decrease the DNA-binding ability, confirming the significant and conserved roles that these residues play in ParB homologues.

ACKNOWLEDGMENTS

We thank Tim R. Dafforn, University of Birmingham, School of Biosciences, for guidance in the analytical ultracentrifugation (AUC) technique and Joanna Zylinska, Institute of Biochemistry and Biophysics, Microbial Biochemistry Department, for assistance in plasmid sequencing.

This study was funded by Wellcome Trust Collaborative Research Initiative grant 067068/Z/02/Z and in part by an EMBO short-term fellowship (ASTF 176.00.06) awarded to M.K. and MNiSW grant 2913/B/PO1/2008/34.

REFERENCES

1. **Adachi, S., K. Hori, and S. Hiraga.** 2006. Subcellular positioning of F plasmid mediated by dynamic localization of SopA and SopB. J. Mol. Biol. **356:**850–863.
2. **Arnold, K., L. Bordoli, J. Kopp, and T. Schwede.** 2006. The Swiss-MODEL workspace: a web-based environment for protein structure homology modeling. Bioinformatics **22:**195–201.
3. **Autret, S., R. Nair, and J. Errington.** 2001. Genetic analysis of the chromosome segregation protein Spo0J of *Bacillus subtilis*: evidence for separate domains involved in DNA binding and interactions with Soj protein. Mol. Microbiol. **41:**743–755.
4. **Bartosik, A. A., J. Mierzejewska, C. M. Thomas, and G. Jagura-Burdzy.** 2009. ParB deficiency in *Pseudomonas aeruginosa* destabilizes the partner protein ParA and affects a variety of physiological parameters. Microbiology **155:**1080–1092.
5. **Bartosik, A. A., K. Lasocki, J. Mierzejewska, C. M. Thomas, and G. Jagura-Burdzy.** 2004. ParB of *Pseudomonas aeruginosa*: interactions with its partner ParA and its target *parS* and specific effects on bacterial growth. J. Bacteriol. **186:**6983–6998.
6. **Bingle, L. E., D. P. Macartney, A. Fantozzi, S. E. Manzoor, and C. M. Thomas.** 2005. Flexibility in repression and cooperativity by KorB of broad host range IncP-1 plasmid RK2. J. Mol. Biol. **349:**302–316.
7. **Breier, A. M., and A. D. Grossman.** 2007. Whole-genome analysis of the chromosome partitioning and sporulation protein Spo0J (ParB) reveals spreading and origin-distal sites on the *Bacillus subtilis* chromosome. Mol. Microbiol. **64:**703–718.
8. **Cervin, M. A., et al.** 1998. A negative regulator linking chromosome segregation to developmental transcription in *Bacillus subtilis*. Mol. Microbiol. **29:**85–95.
9. **Churchward, G., D. Belin, and Y. A. Nagamine.** 1984. pSC101-derived plasmid which shows no sequence homology to other commonly used cloning vectors. Gene **31:**165–171.
10. **Delbrück, H., G. Ziegelin, E. Lanka, and U. Heinemann.** 2002. An Src homology 3-like domain is responsible for dimerization of the repressor protein KorB encoded by the promiscuous IncP plasmid RP4. J. Biol. Chem. **277:**4191–4198.
11. **El-Sayed, A. K., J. Hothersall, and C. M. Thomas.** 2001. Quorum-sensing-dependent regulation of biosynthesis of the polyketide antibiotic mupirocin in *Pseudomonas fluorescens* NCIMB 10586. Microbiology **147:**2127–2139.
12. **Gerdes, K., J. Moller-Jensen, and R. Bugge Jensen.** 2000. Plasmid and chromosome partitioning: surprises from phylogeny. Mol. Microbiol. **37:**455–466.
13. **Gerdes, K., M. Howard, and F. Szardenings.** 2010. Pushing and pulling in prokaryotic DNA segregation. Cell **141:**927–942.
14. **Godfrin-Estevenon, A.-M., F. Pasta, and D. Lane.** 2002. The *parAB* gene products of *Pseudomonas putida* exhibit partition activity in both *P. putida* and *Escherichia coli*. Mol. Microbiol. **43:**39–49.
15. **Hanahan, D.** 1983. Studies on transformation of *Escherichia coli* with plasmids. J. Mol. Biol. **166:**557–580.
16. **Hanai, R., et al.** 1996. Molecular dissection of a protein SopB essential for *Escherichia coli* F plasmid partition. J. Biol. Chem. **271:**17469–17475.
17. **Hayes, F.** 2000. The partition system of multidrug resistance plasmid TP228 includes a novel protein that epitomizes an evolutionarily distinct subgroup of the ParA superfamily. Mol. Microbiol. **37:**528–541.
18. **Irani, V. R., and J. J. Rowe.** 1997. Enhancement of transformation in *Pseudomonas aeruginosa* PAO1 by Mg^{2+} and heat. Biotechniques **22:**54–56.
19. **Ireton, K., and A. D. Grossman.** 1994. A developmental checkpoint couples the initiation of sporulation to DNA replication in *Bacillus subtilis*. EMBO J. **13:**1566–1573.
20. **Jagura-Burdzy, G., and C. M. Thomas.** 1995. Purification of KorA protein from broad host range plasmid RK2: definition of a hierarchy of KorA operators. J. Mol. Biol. **253:**39–50.
21. **Jagura-Burdzy, G., et al.** 1999. Repression at a distance by the global regulator KorB of promiscuous IncP plasmids. Mol. Microbiol. **32:**519–532.
22. **Jagura-Burdzy, G., J. P. Ibbotson, and C. M. Thomas.** 1991. The *korF* region of broad-host-range plasmid RK2 encodes two polypeptides with transcriptional repressor activity. J. Bacteriol. **173:**826–833.
23. **Jakimowicz, D., B. Gust, J. Zakrzewska-Czerwinska, and K. F. Chater.** 2005. Developmental-stage-specific assembly of ParB complexes in *Streptomyces coelicolor* hyphae. J. Bacteriol. **187:**3572–3580.
24. **Jakimowicz, D., K. Chater, and J. Zakrzewska-Czerwínska.** 2002. The ParB protein of *Streptomyces coelicolor* A3(2) recognizes a cluster of *parS* sequences within the origin-proximal region of the linear chromosome. Mol. Microbiol. **45:**1365–1377.
25. **Kahn, M., et al.** 1979. Plasmid cloning vehicles derived from plasmids ColE1, F, R6K, and RK2. Methods Enzymol. **68:**268–280.
26. **Khare, D., G. Ziegelin, E. Lanka, and U. Heinemann.** 2004. Sequence-specific DNA binding determined by contacts outside the helix-turn-helix motif of the ParB homolog KorB. Nat. Struct. Mol. Biol. **11:**656–663.
27. **Kois, A., M. Swiatek, D. Jakimowicz, and J. Zakrzewska-Czerwińska.** 2009. SMC protein-dependent chromosome condensation during aerial hyphal development in *Streptomyces*. J. Bacteriol. **191:**310–319.
28. **Kovach, M. E., et al.** 1995. Four new derivatives of the broad-host-range cloning vector pBBR1MCS1, carrying different antibiotic-resistance cassettes. Gene **166:**175–176.
29. **Larsen, R. A., et al.** 2007. Treadmilling of a prokaryotic tubulin-like protein, TubZ, required for plasmid stability in *Bacillus thuringiensis*. Genes Dev. **21:**1340–1352.
30. **Lasocki, K., A. A. Bartosik, J. Mierzejewska, C. M. Thomas, and G. Jagura-Burdzy.** 2007. Deletion of the *parA* (*soj*) homologue in *Pseudomonas aeruginosa* causes ParB instability and affects growth rate, chromosome segregation, and motility. J. Bacteriol. **189:**5762–5772.
31. **Lee, P. S., D. C.-H. Lin, S. Moriya, and A. D. Grossman.** 2003. Effects of the chromosome partitioning protein Spo0J (ParB) on *oriC* positioning and replication initiation in *Bacillus subtilis*. J. Bacteriol. **185:**1326–1337.
32. **Leonard, T. A., P. J. Butler, and J. Löwe.** 2004. Structural analysis of the chromosome segregation protein Spo0J from *Thermus thermophilus*. Mol. Microbiol. **53:**419–432.
33. **Lewis, R. A., C. R. Bignell, W. Zeng, A. C. Jones, and C. M. Thomas.** 2002. Chromosome loss from par mutants of *Pseudomonas putida* depends on growth medium and phase of growth. Microbiology **148:**537–548.
34. **Livny, J., Y. Yamaichi, and M. K. Waldor.** 2007. Distribution of centromere-like *parS* sites in bacteria: insights from comparative genomics. J. Bacteriol. **189:**8693–8703.
35. **Lobocka, M., and M. Yarmolinsky.** 1996. P1 plasmid partition: a mutational analysis of ParB. J. Mol. Biol. **259:**366–382.
36. **Lukaszewicz, M., et al.** 2002. Functional dissection of the ParB homologue (KorB) from IncP-1 plasmid RK2. Nucleic Acids Res. **30:**1046–1055.
37. **Lynch, A. S., and J. C. Wang.** 1995. SopB protein-mediated silencing of genes linked to the *sopC* locus of *Escherichia coli* F plasmid. Proc. Natl. Acad. Sci. U. S. A. **92:**1896–1900.
38. **Mohl, D. A., and J. W. Gober.** 1997. Cell-cycle dependent polar localization of chromosome partitioning proteins in *Caulobacter crescentus*. Cell **88:**675–684.
39. **Mohl, D. A., J. Easter, Jr., and J. W. Gober.** 2001. The chromosome parti-

tioning protein, ParB, is required for cytokinesis in *Caulobacter crescentus*. Mol. Microbiol. **42:**741–755.
40. **Mori, H., et al.** 1989. Purification and characterization of SopA and SopB proteins essential for F plasmid partitioning. J. Biol. Chem. **264:**15535–15541.
41. **Murray, H., and J. Errington.** 2008. Dynamic control of the DNA replication initiation protein DnaA by Soj/ParA. Cell **135:**74–84.
42. **Pansegrau, W., et al.** 1994. Complete nucleotide sequence of Birmingham IncP alpha plasmids. Compilation and comparative analysis. J. Mol. Biol. **239:**623–663.
43. **Rashid, M. H., and A. Kornberg.** 2000. Inorganic polyphosphate is needed for swimming, swarming, and twitching motilities of *Pseudomonas aeruginosa*. Proc. Natl. Acad. Sci. U. S. A. **97:**4885–4890.
44. **Rodionov, O., M. Lobocka, and M. Yarmolinsky.** 1999. Silencing of genes flanking the P1 plasmid centromere. Science **283:**546–549.
45. **Sambrook, J., E. F. Fritsch, and T. Maniatis.** 1989. Molecular cloning: a laboratory manual, 2nd ed. Cold Spring Harbor Laboratory Press, Cold Spring Harbor, NY.
46. **Schuck, P.** 2000. Size-distribution analysis of macromolecules by sedimentation velocity ultracentrifugation and Lamm equation modeling. Biophys. J. **78:**1606–1919.
47. **Schumacher, M. A., and B. E. Funnell.** 2005. Structures of ParB bound to DNA reveal mechanism of partition complex formation. Nature **438:**516–519.
48. **Schumacher, M. A., K. M. Piro, and W. Xu.** 2010. Insight into F plasmid DNA segregation revealed by structures of SopB and SopB-DNA complexes. Nucleic Acids Res. **38:**4514–4526.
49. **Schwede, T., J. Kopp, N. Guex, and M. C. Peitsch.** 2003. SWISS-MODEL: an automated protein homology-modeling server. Nucleic Acids Res. **31:**3381–3385.
50. **Simon, R., M. O'Connell, M. Labes, and A. Puhler.** 1986. Plasmid vectors for the genetic analysis and manipulation of *Rhizobia* and other gram-negative bacteria. Methods Enzymol. **118:**640–659.
51. **Simpson, A. E., R. A. Skurray, and N. Firth.** 2003. A single gene on the staphylococcal multiresistance plasmid pSK1 encodes a novel partitioning system. J. Bacteriol. **185:**2143–2152.
52. **Surtees, J. A., and B. E. Funnell.** 1999. P1 ParB domain structure includes two independent multimerization domains. J. Bacteriol. **181:**5898–5908.
53. **Surtees, J. A., and B. E. Funnell.** 2001. The DNA binding domains of P1 ParB and the architecture of the P1 plasmid partition complex. J. Biol. Chem. **276:**12385–12394.
54. **Yamaichi, Y., and H. Niki.** 2000. Active segregation by the *Bacillus subtilis* partitioning system in *Escherichia coli*. Proc. Natl. Acad. Sci. U. S. A. **97:**14656–14661.
55. **Yamaichi, Y., M. A. Fogel, S. M. McLeod, M. P. Hui, and M. K. Waldor.** 2007. Distinct centromere-like *parS* sites on the two chromosomes of *Vibrio* spp. J. Bacteriol. **189:**5314–5324.
56. **Ye, Y., and A. Godzik.** 2004. FATCAT: a web server for flexible structure comparison and structure similarity searching. Nucleic Acids Res. **32**(web server issue)**:**W582–W585.